

## Supporting Information

### Optical Readout of Controlled Monomer-Dimer Self-Assembly

P. A. Tarakanov,<sup>\*ab</sup> E. N. Tarakanova,<sup>a</sup> P. V. Dorovatovskii,<sup>c</sup> Y. V. Zubavichus,<sup>c</sup> V. N. Khrustalev,<sup>d</sup>  
S. A. Trashin,<sup>ae</sup> K. De Wael,<sup>c</sup> M. E. Neganova,<sup>a</sup> D. V. Mischenko,<sup>b</sup> J. L. Sessler,<sup>f</sup> P. A. Stuzhin,<sup>g</sup>  
V. E. Pushkarev<sup>\*ah</sup> and L. G. Tomilova<sup>ah</sup>

<sup>a</sup> Institute of Physiologically Active Compounds, Russian Academy of Sciences, 1 Severny Proezd, 142432 Chernogolovka, Moscow Region, Russian Federation. E-mails: tarakanov\_pa@ipac.ac.ru; pushkarev@ipac.ac.ru

<sup>b</sup> Institute of Problems of Chemical Physics, Russian Academy of Sciences, 1 Academician Semenov Avenue, 142432 Chernogolovka, Moscow Region, Russian Federation

<sup>c</sup> National Research Centre “Kurchatov Institute”, 1 Akad. Kurchatov Sq., Moscow 123182, Russia

<sup>d</sup> Inorganic Chemistry Department, Peoples’ Friendship University of Russia (RUDN University), 6 Miklukho-Maklay St., Moscow 117198, Russian Federation

<sup>e</sup> AXES Research Group, Department of Chemistry, University of Antwerp, Groenenborgerlaan 171, 2020 Antwerpen, Belgium

<sup>f</sup> Department of Chemistry, Shanghai University, Shanghai 200444, China

<sup>g</sup> Research Institute of Macroheterocycles, Ivanovo State University of Chemistry and Technology, 153000 Ivanovo, Russia

<sup>h</sup> Department of Chemistry, M.V. Lomonosov Moscow State University, 1 Leninskie Gory, 119991 Moscow, Russian Federation

### Table of Contents

General Information	S2
Synthesis	S2
NMR Spectra	S3
X-ray Diffraction Analysis	S9
Studies of the Extent of Dissociation	S11
Studies of the Influence of Fluoride Ion Concentration on the Dimer-Monomer Equilibria	S12
Electrochemistry	S19
<i>In Vitro</i> and <i>in Vivo</i> Toxicity Tests	S21
References	S21

## General Information

UV-vis spectra were recorded on a Hitachi U-2900 spectrophotometer using quartz cuvettes (10 × 10 mm) with the samples dissolved in pyridine, DMSO, *o*-DCB, unless otherwise specified. <sup>1</sup>H and <sup>13</sup>C NMR spectra were recorded on Bruker Avance 500 (500 and 125 MHz, respectively) with the samples dissolved in pyridine-*d*<sub>5</sub> or DMSO-*d*<sub>6</sub>. Chemical shifts are given in parts per million (ppm) relative to TMS. Matrix-assisted laser desorption/ionization time-of-flight (MALDI-TOF) mass spectra were acquired on a VISION-2000 mass spectrometer with  $\alpha$ -cyano-4-hydroxycinnamic acid (CHCA) as the matrix. Size exclusion column chromatography was carried out using Bio-Beads S-X1 resin (BIORAD) eluted with pyridine. All other reagents and solvents were obtained or distilled according to standard procedures. All reactions were controlled by TLC and UV-vis until complete disappearance of the starting materials, unless otherwise specified.

Electrochemical measurements were carried out in pyridine using a conventional three-electrode cell and Autolab/PGSTAT101 (Metrohm Autolab B.V., the Netherlands). A double junction Ag/AgCl reference electrode (Metrohm, Switzerland) was filled with 2 M LiCl in ethanol as the reference (inner) electrolyte and 0.1 M [TBA][BF<sub>4</sub>] in pyridine as the bridge electrolyte. Before making any measurements, a platinum disk working electrode (2 mm in diameter, BASi, USA) was regenerated by polishing with an abrasive paper (grit 400), washed with ultrapure water and drying. Blank voltammograms were recorded in pure pyridine containing 0.1 M [TBA][BF<sub>4</sub>] and then approximately 1 mM of a sample was introduced into the cell. After a series of measurements, ferrocene was added as internal reference, and additional voltammograms were recorded. Before the measurements the solutions were purged with N<sub>2</sub> for at least 30 min. All measurements were performed at room temperature (22 ± 2°C).

## Synthesis

**General procedure for the preparation of complexes 2a,b.** Mg metal (50 mg) was boiled in isoamyl alcohol (50 mL) in the presence of a catalytic amount of I<sub>2</sub> until complete dissolution was observed (ca. 3 h). The solution of the resulting Mg alkoxide was cooled to room temperature, 1,4-diazepine-2,3-dicarbonitrile **1a** or **1b** (1 mmol) was added, and the mixture was heated at reflux for 16 h. The course of the reaction was monitored by UV-vis spectroscopy. Then, the reaction mixture was cooled to room temperature and the solvent was evaporated under reduced pressure. The resulting dry residue was successively washed with 50% aqueous acetic acid (4 × 50 mL), a 5% aqueous solution of sodium bicarbonate (2 × 50 mL), distilled water (4 × 50 mL) and finally with MeOH (50 mL) followed by drying *in vacuo* at 50 °C. The resulting solid was subjected to gel permeation chromatography (Bio-Beads S-X1, pyridine). This yielded **2a** and **2b** in the form of dark-green solids.

**Tetrakis{5,7-bis[2'-(4-bromophenyl)ethenyl]-6H-1,4-diazepino}[2,3-*b,g,l,q*]porphyrazinato magnesium (II) (**2a**).** Yield 0.44 g (86%). UV-vis (DMSO)  $\lambda_{\text{max}}/\text{nm}$  (log  $\epsilon$ ): 387 (4.77), 659 (4.59), 700 (4.41). <sup>1</sup>H NMR (500 MHz; DMSO-*d*<sub>6</sub>)  $\delta/\text{ppm}$ : 8.20 (8H, d, <sup>3</sup>*J* = 15.9 Hz, 2'-H), 7.7–7.65 (24H, br m, 1'-H; H<sup>*o*-Ar</sup>), 7.47 (16H, br s, H<sup>*m*-Ar</sup>), 6.11 (4H, br s, H<sup>eq</sup>), 4.77 (4H, br s, H<sup>ax</sup>). <sup>13</sup>C NMR (125 MHz; Py-*d*<sub>5</sub>)  $\delta/\text{ppm}$ : 154.99, 149.19, 143.05, 137.46, 132.50, 131.68, 129.82, 37.75. MS (MALDI-TOF; HCCA): *m/z* 2050.87 [*M*+H]<sup>+</sup>, 4101.46 [*M*<sub>2</sub>+H]<sup>+</sup>; calculated for C<sub>92</sub>H<sub>57</sub>Br<sub>8</sub>MgN<sub>16</sub>: 2050.82.

**Tetrakis{5,7-bis[2'-(4-methoxyphenyl)ethenyl]-6H-1,4-diazepino}[2,3-*b,g,l,q*]porphyrazinato magnesium(II) (**2b**).** Yield 0.39 g (94%). UV-vis (DMSO)  $\lambda_{\text{max}}/\text{nm}$  (log  $\epsilon$ ): 386 (5.05), 661 (4.87), 698 (4.78). <sup>1</sup>H NMR (500 MHz; pyridine-*d*<sub>5</sub>)  $\delta/\text{ppm}$ : 8.49 (8H, d, <sup>3</sup>*J* = 16.53 Hz, 2'-H), 8.13 (8H, d, <sup>3</sup>*J* = 16.06 Hz, 1'-H), 7.69 (16H, d, <sup>3</sup>*J* = 7.79 Hz, H<sup>*o*-Ar</sup>), 6.89 (16H, d, <sup>3</sup>*J* = 8.15 Hz, H<sup>*m*-Ar</sup>), 6.67 (4H, br s, H<sup>eq</sup>), 5.94 (4H, d, <sup>2</sup>*J* = 12.64 Hz, H<sup>ax</sup>), 3.81 (24H, s, -OMe). <sup>13</sup>C NMR (125 MHz; Py-*d*<sub>5</sub>)  $\delta/\text{ppm}$ : 161.12, 154.86, 143.05, 138.65, 130.15, 130.03, 128.95, 114.99, 55.62, 38.48. MS (MALDI-TOF/TOF; HCCA): *m/z* 1658.60 [*M*+H]<sup>+</sup>, 3317.07 [*M*<sub>2</sub>+H]<sup>+</sup>; calculated for C<sub>100</sub>H<sub>81</sub>MgN<sub>16</sub>O<sub>8</sub>: 1658.63.

**Tetrakis(5,7-bis(4-*tert*-butylphenyl)-6H-1,4-diazepino)[2,3-*b,g,l,q*]porphyrazinato magnesium(II) (**2c**)** was synthesized according to a previously published procedure.<sup>1</sup>

## NMR Spectra

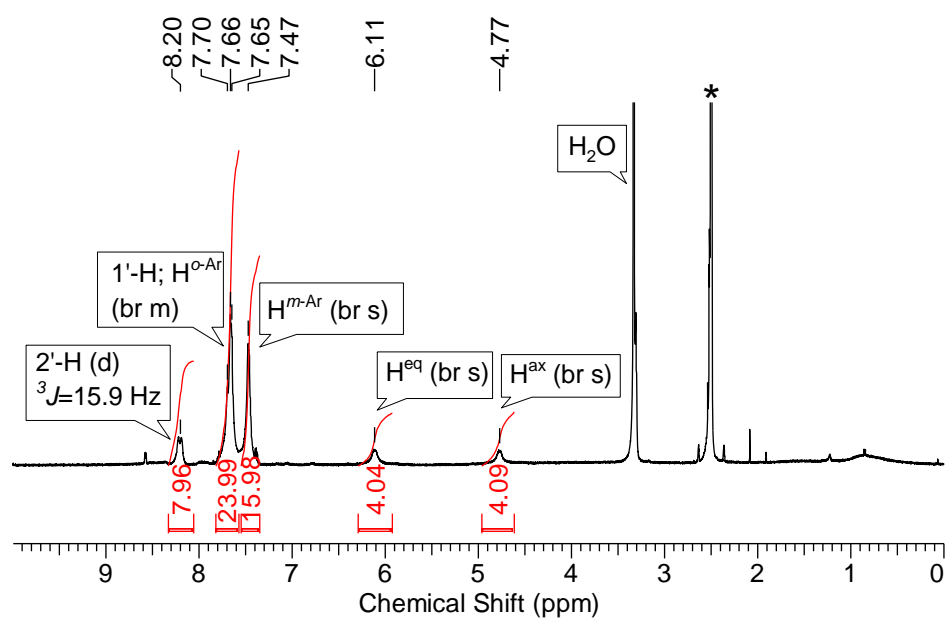


Figure S1.  $^1\text{H}$  NMR spectrum of **2a** (DMSO- $d_6$ , 293 K).

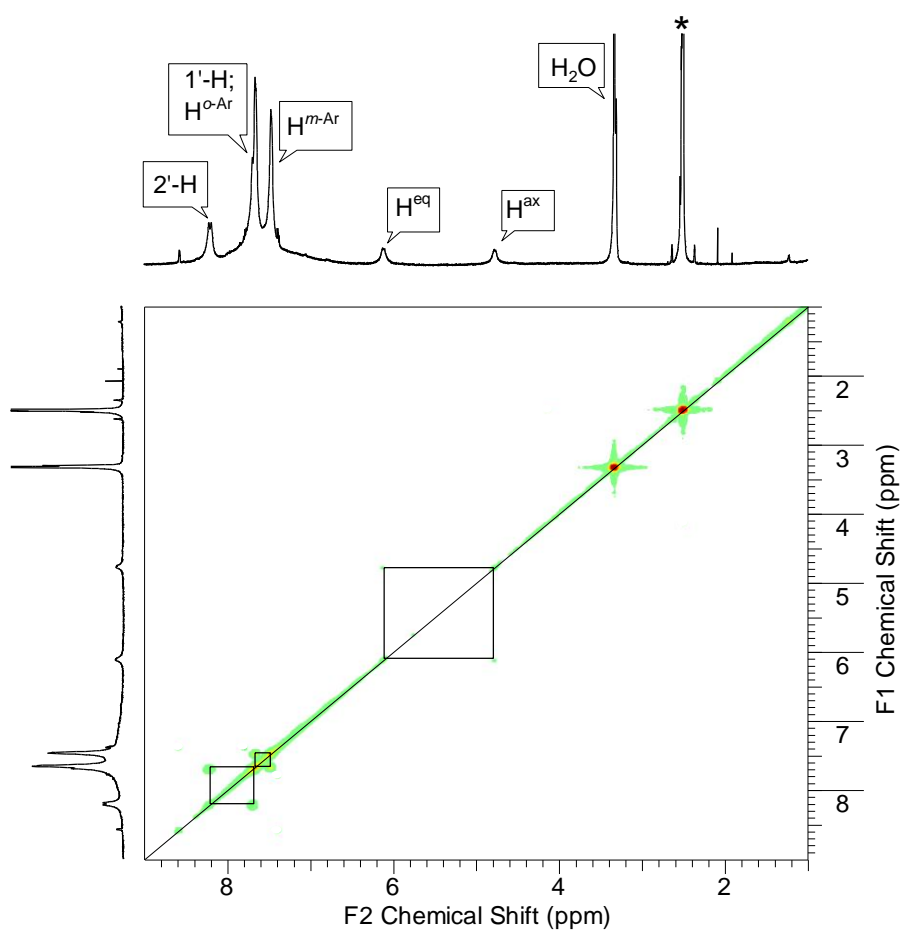
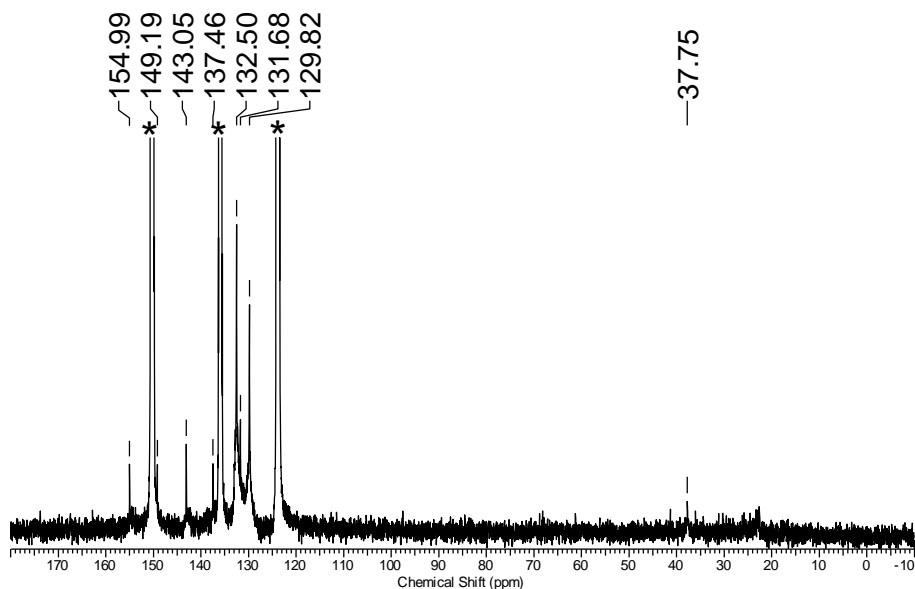
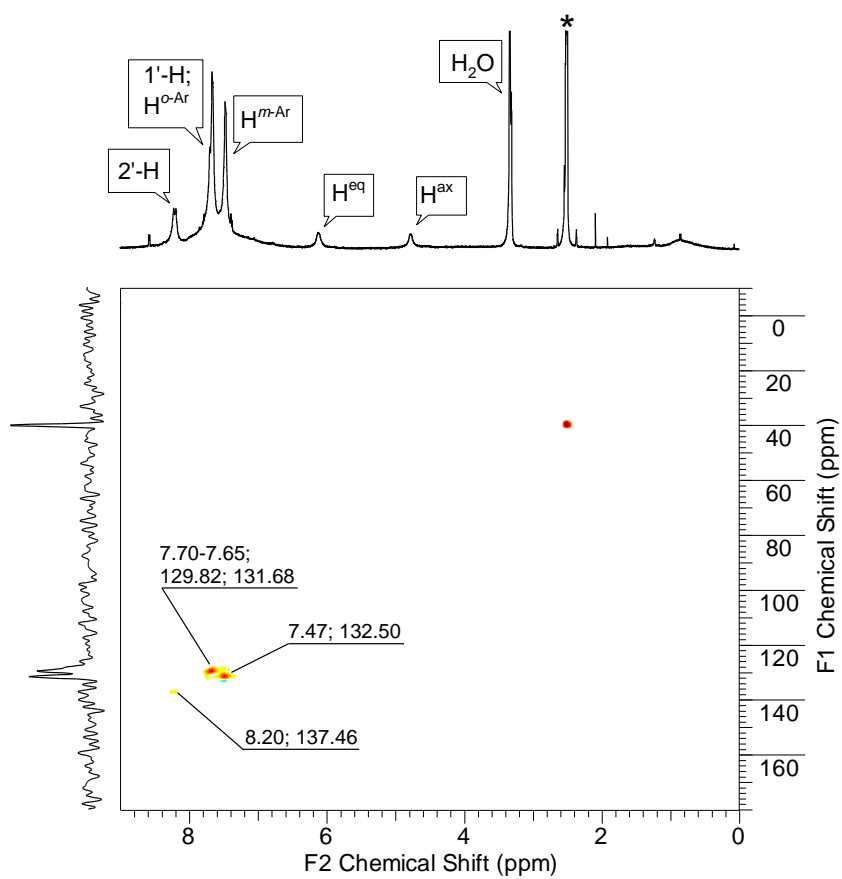


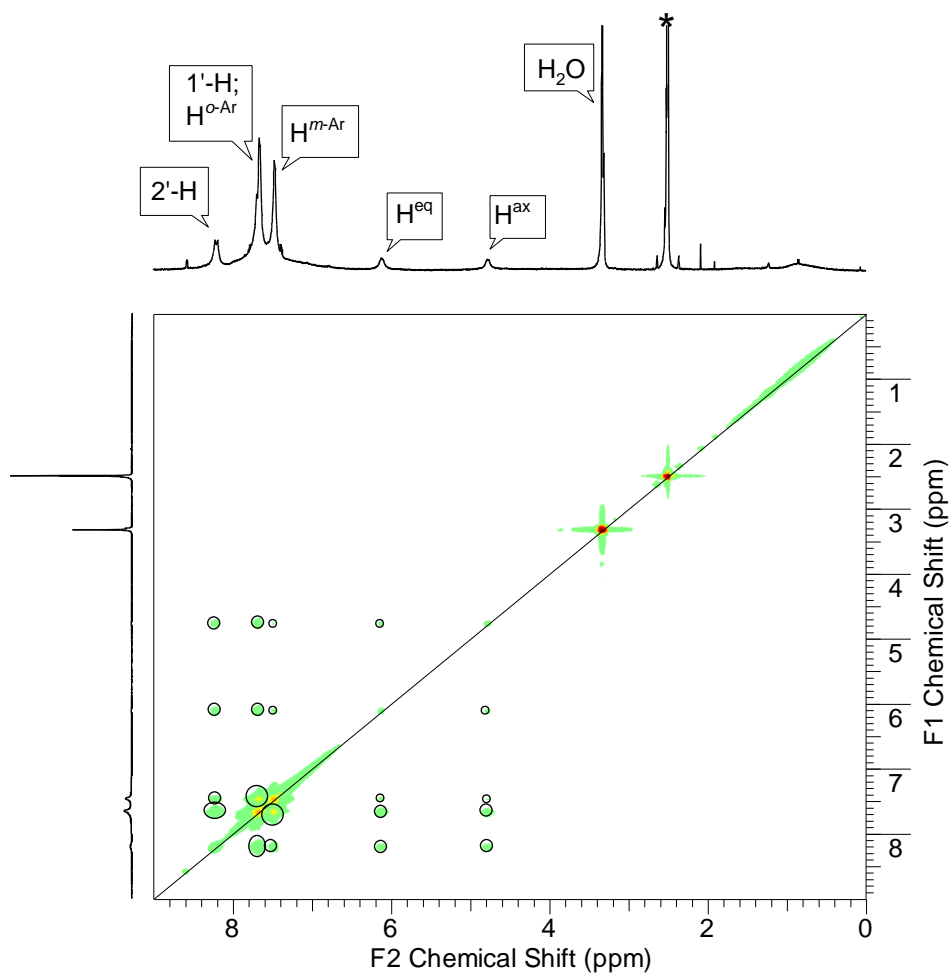
Figure S2.  $^1\text{H}$ - $^1\text{H}$  COSY NMR spectrum of **2a** (DMSO- $d_6$ , 293 K).



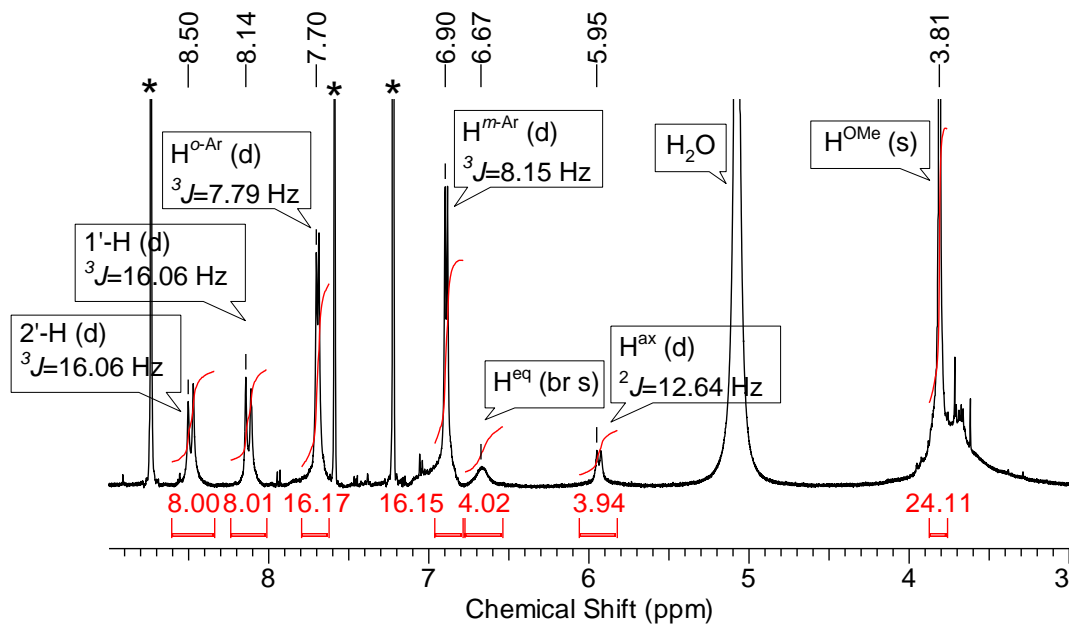
**Figure S3.**  $^{13}\text{C}$  NMR spectrum of **2a** (pyridine- $d_5$ , 293 K).



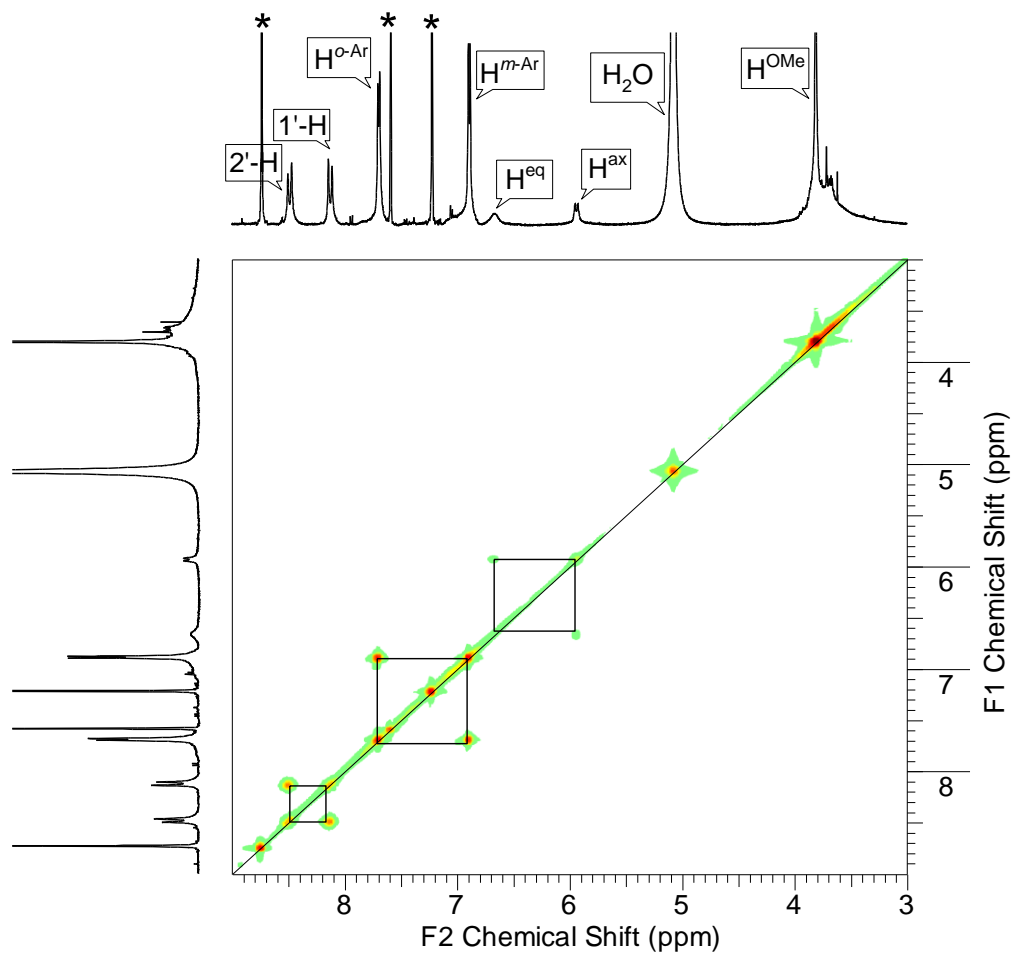
**Figure S4.**  $^1\text{H}$ - $^{13}\text{C}$  HSQC spectrum of **2a** (DMSO- $d_6$ , 293 K).



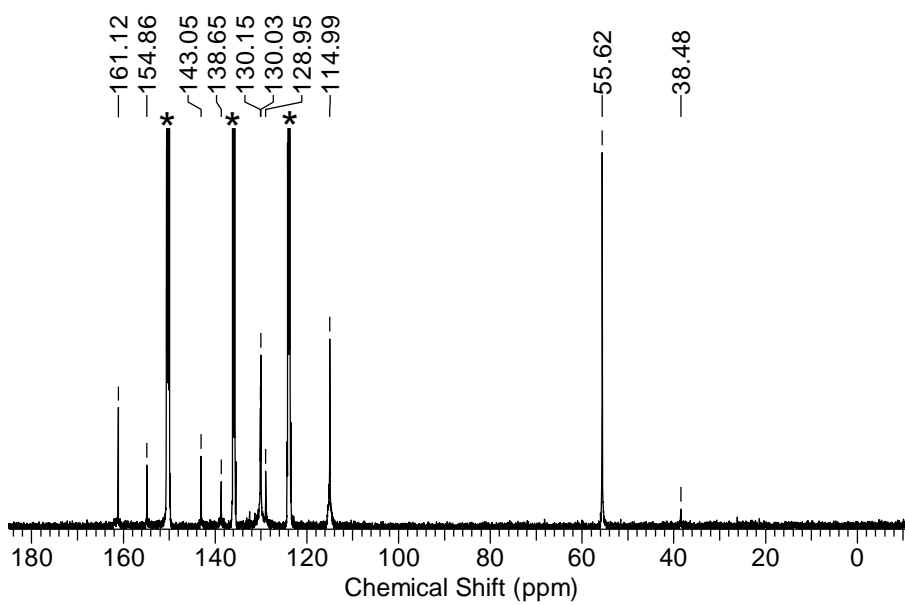
**Figure S5.**  $^1\text{H}$ - $^1\text{H}$  NOESY spectrum of **2a** (DMSO- $d_6$ , 293 K).



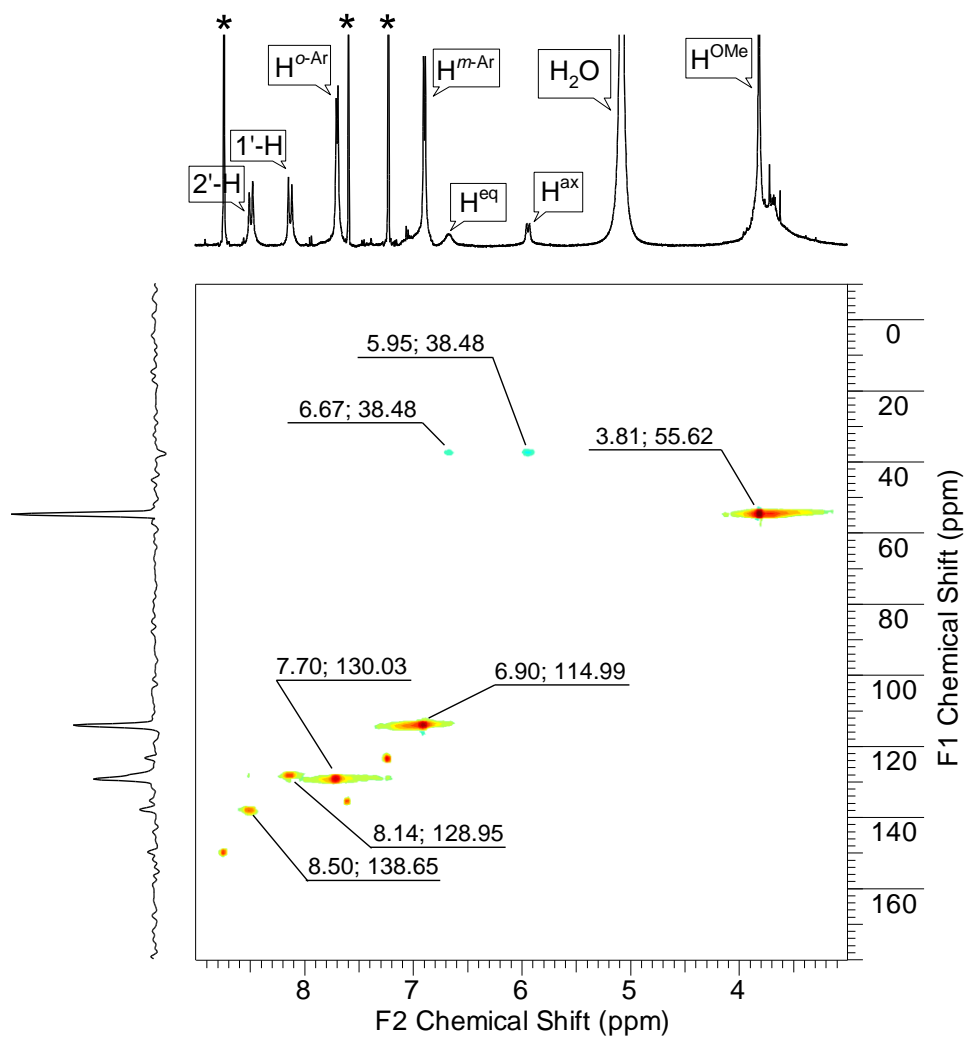
**Figure S6.**  $^1\text{H}$  NMR spectrum of **2b** (pyridine- $d_5$ , 293 K).



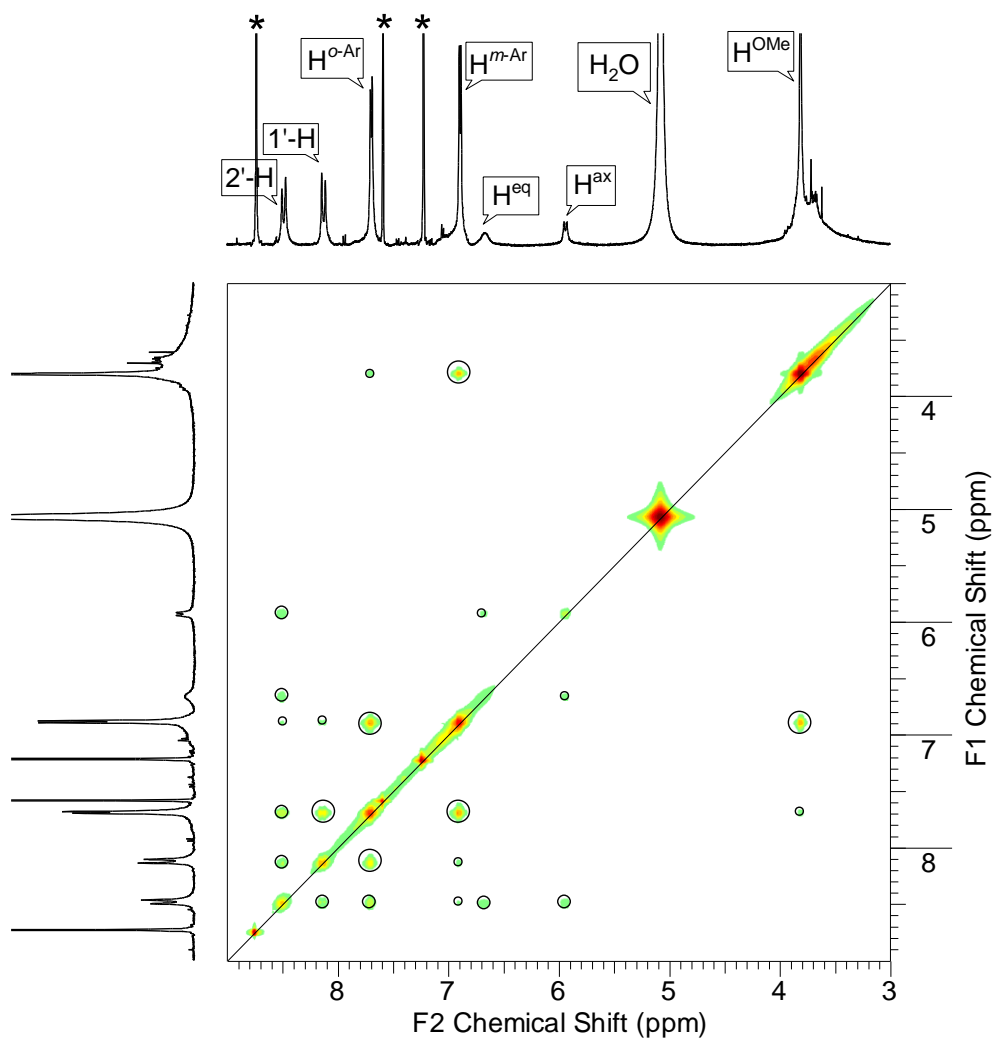
**Figure S7.**  $^1\text{H}$ - $^1\text{H}$  COSY NMR spectrum of **2b** (pyridine- $d_5$ , 293 K).



**Figure S8.**  $^{13}\text{C}$  NMR spectrum of **2b** (pyridine- $d_5$ , 293 K).



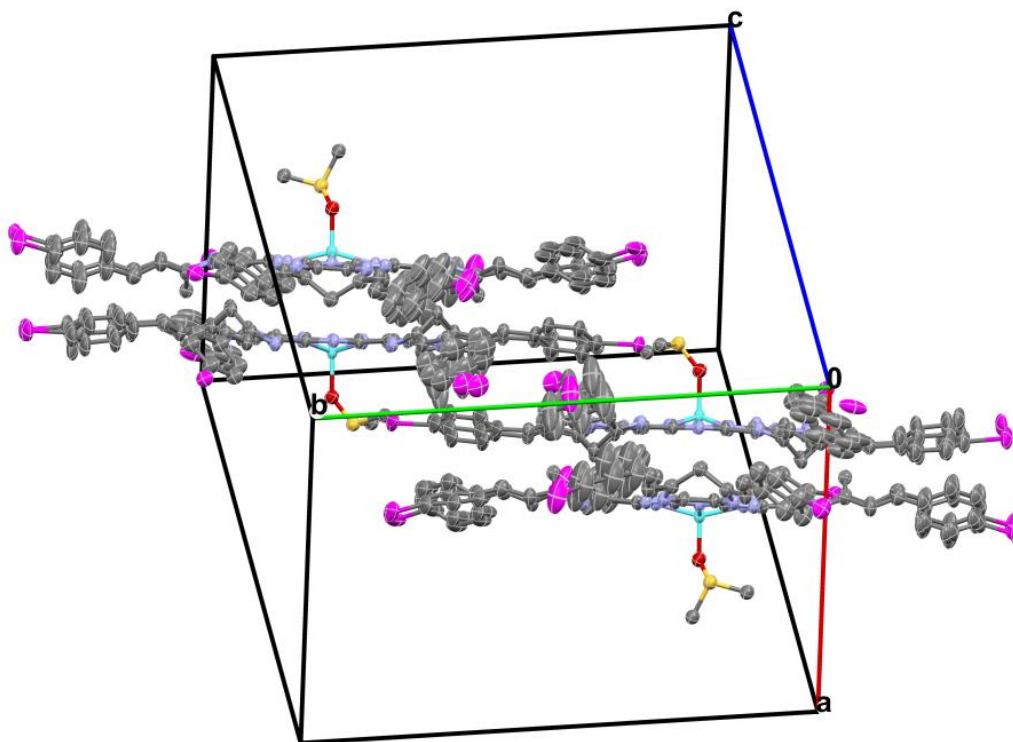
**Figure S9.**  $^1\text{H}$ - $^{13}\text{C}$  HSQC spectrum of **2b** (pyridine- $d_5$ , 293 K).



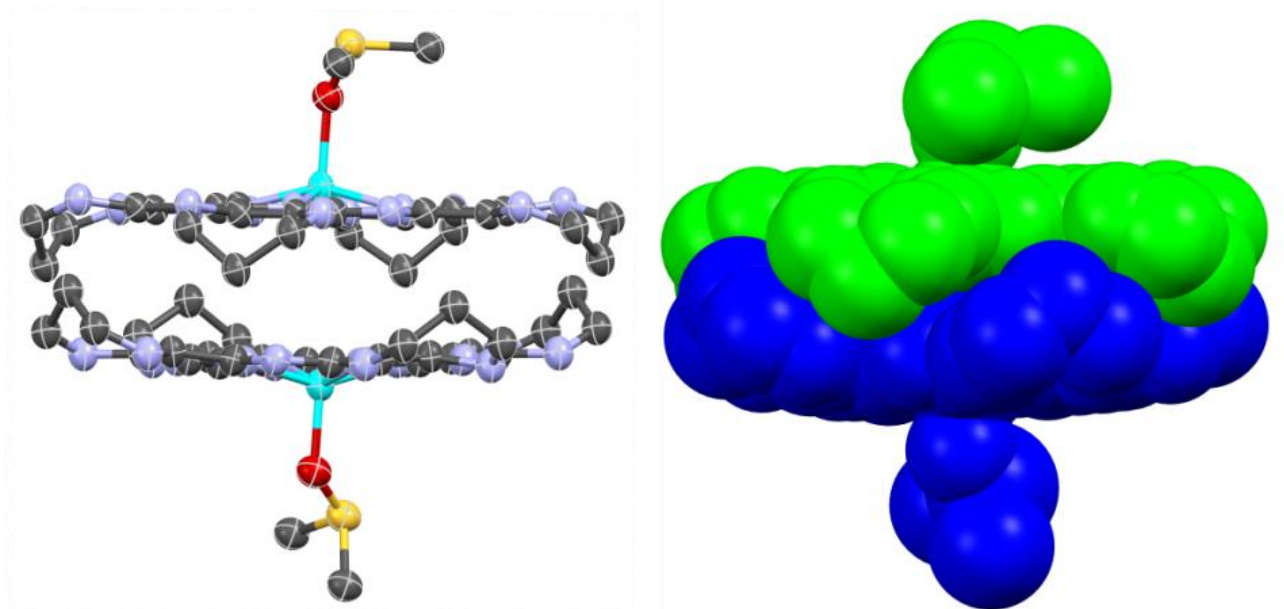
**Figure S10.**  $^1\text{H}$ - $^1\text{H}$  NOESY spectrum of **2b** (pyridine- $d_5$ , 293 K).

## X-ray Diffraction Analysis

The crystal of **2a** ( $C_{94}H_{62}N_{16}OSMgBr_8$ ,  $M = 2127.16$ ) used for study was triclinic, space group  $P-1$ , at  $T = 100$  K:  $a = 15.325(3)$  Å,  $b = 27.895(6)$  Å,  $c = 33.306(7)$  Å,  $\alpha = 113.35(3)^\circ$ ,  $\beta = 100.91(3)^\circ$ ,  $\gamma = 95.58(3)^\circ$ ,  $V = 12599(6)$  Å<sup>3</sup>,  $Z = 4$ ,  $d_{\text{calc}} = 1.121$  g/cm<sup>3</sup>,  $F(000) = 4216$ ,  $\mu = 0.973$  mm<sup>-1</sup>. The X-ray diffraction study was carried out on the 'Belok' beamline ( $\lambda = 0.96990$  Å) of the National Research Center "Kurchatov Institute" (Moscow, Russian Federation) using a Rayonix SX-165 CCD detector. A total of 720 images (117852 reflections, 40519 independent reflections,  $R_{\text{int}} = 0.0851$ ) were collected using an oscillation range of  $1.0^\circ$  ( $\varphi$  scan mode,  $2\theta_{\text{max}} = 76.44^\circ$ ) and corrected for absorption using the *Scala* program ( $T_{\text{min}} = 0.848$ ;  $T_{\text{max}} = 0.898$ ).<sup>2</sup> The data were indexed, integrated and scaled using the utility *iMOSFLM* in CCP4 program.<sup>3</sup> The structure was determined by direct methods and refined by full-matrix least squares technique on  $F^2$  with anisotropic displacement parameters for non-hydrogen atoms. Twelve of the sixteen *para*-bromophenyl substituents were disordered over two sites each with equal occupancies. The independent part of the unit cell of **2a** contained several dimethylsulfoxide and water solvate molecules, which were strongly disordered. All attempts to model and refine their positions were unsuccessful. Therefore, the contribution to the scattering by the solvent molecules was removed by use of the utility *SQUEEZE* in *PLATON06*.<sup>4</sup> The hydrogen atoms were placed in calculated positions and refined within a riding model with fixed isotropic displacement parameters [ $U_{\text{iso}}(\text{H}) = 1.5U_{\text{eq}}(\text{C})$  for the methyl groups and  $1.2U_{\text{eq}}(\text{C})$  for the other groups]. The final divergence factors were  $R_1 = 0.1361$  for 15689 independent reflections with  $I > 2\sigma(I)$  and  $wR_2 = 0.2672$  for all independent reflections,  $S = 1.080$ . The calculations were performed using the *SHELXTL* program.<sup>5</sup> Full crystallographic data for the investigated compounds have been deposited with the Cambridge Crystallographic Data Center, CCDC 1489687. Copies of this information may be obtained free of charge from the Director, CCDC, 12 Union Road, Cambridge CB2 1EZ, UK (fax: +44 1223 336033; e-mail: [deposit@ccdc.cam.ac.uk](mailto:deposit@ccdc.cam.ac.uk) or [www.ccdc.cam.ac.uk](http://www.ccdc.cam.ac.uk)).

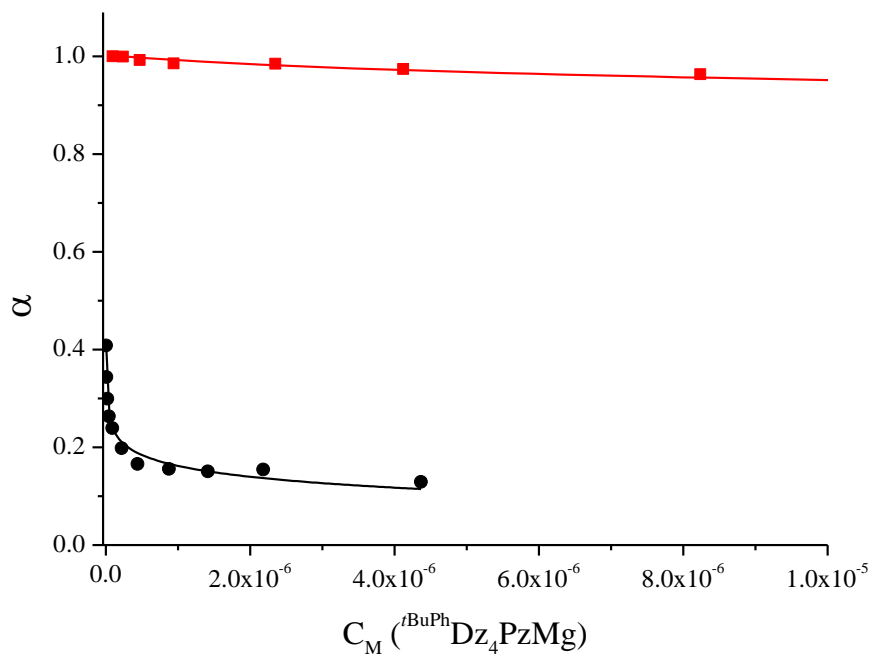


**Figure S11.** X-ray analysis data for **2a**. Show packing of **2a** in the crystal cell (hydrogen atoms are omitted for clarity).

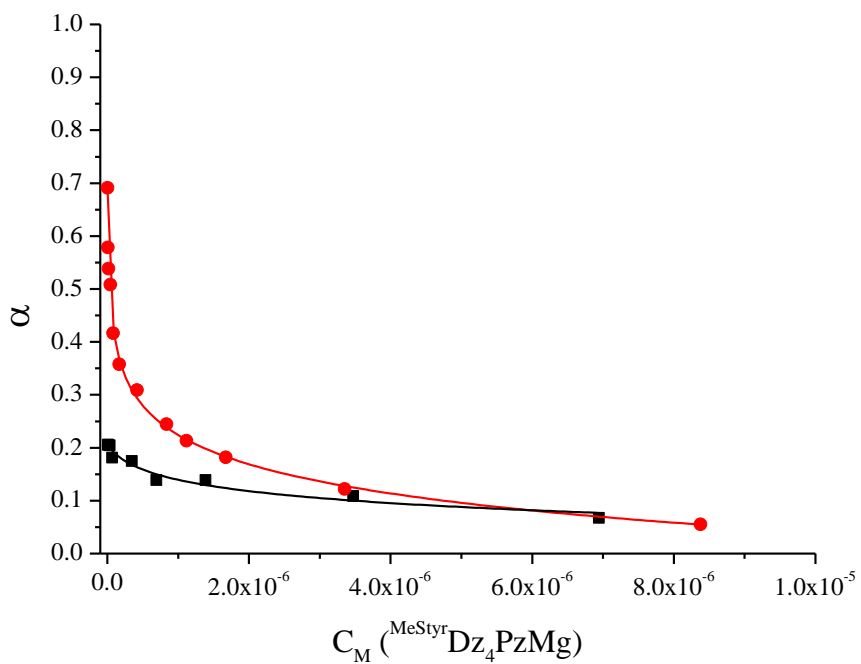


**Figure S12.** Views of the X-ray structure of **2a**. Ellipsoid (left) and space filling (right) representations, respectively (hydrogen atoms and (aryl)ethenyl substituents are omitted for clarity).

## Studies of the Extent of Dissociation



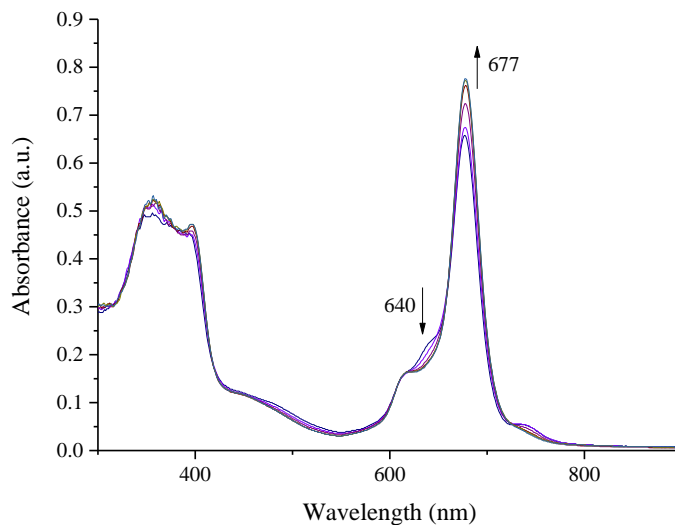
**Figure S13.** The extent of dissociation ( $\alpha$ ) as function of concentration (mol L<sup>-1</sup>) of **2c** in DMSO (red line) and in pyridine (black line).



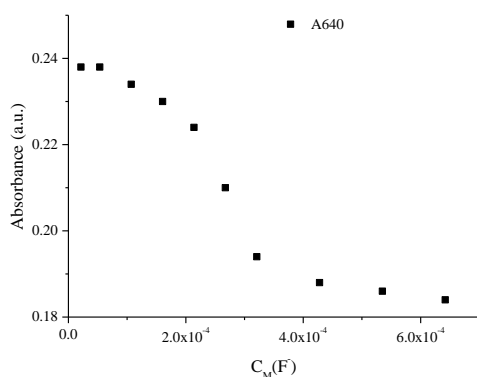
**Figure S14.** The extent of dissociation ( $\alpha$ ) as function of concentration of **2b** (mol L<sup>-1</sup>) in DMSO (red line) and in pyridine (black line).

## Studies of the Influence of Fluoride Ion Concentration on the Dimer-Monomer Equilibria

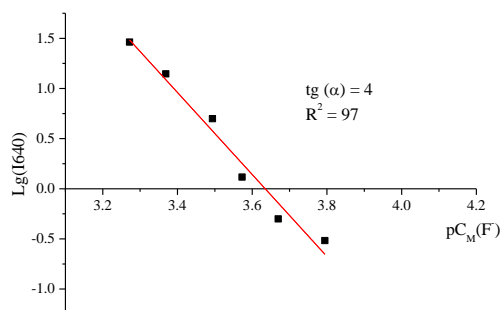
Complex **2c** in DMSO



**Figure S15.** UV-vis spectroscopic changes seen upon addition of tetrabutylammonium fluoride to a solution of **2c** in DMSO.

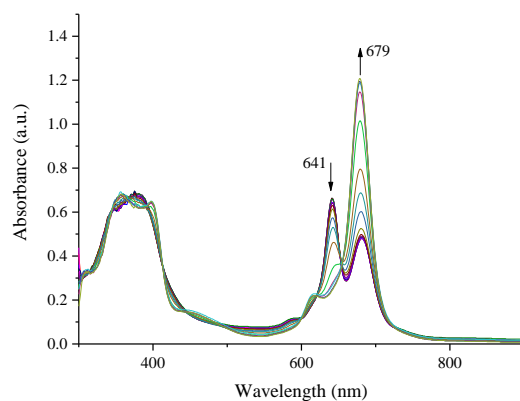


**Figure S16.** Change in absorbance at 640 nm seen upon titration of **2c** with tetrabutylammonium fluoride in DMSO. Concentrations are in mol L<sup>-1</sup>.

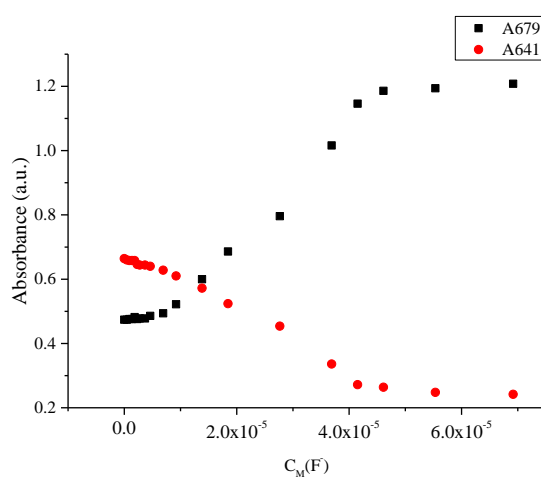


**Figure S17.** Plot of the indicator concentration ratio for **2c** at 640 nm vs. the negative log of the tetrabutylammonium fluoride concentration.

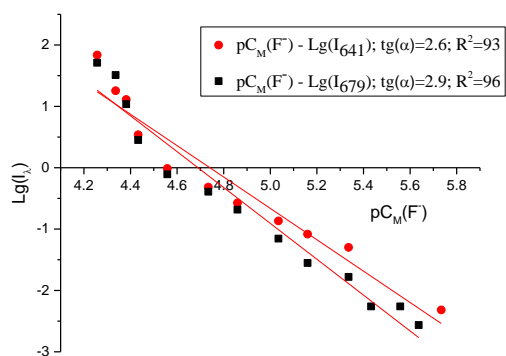
### Complex **2c** in pyridine



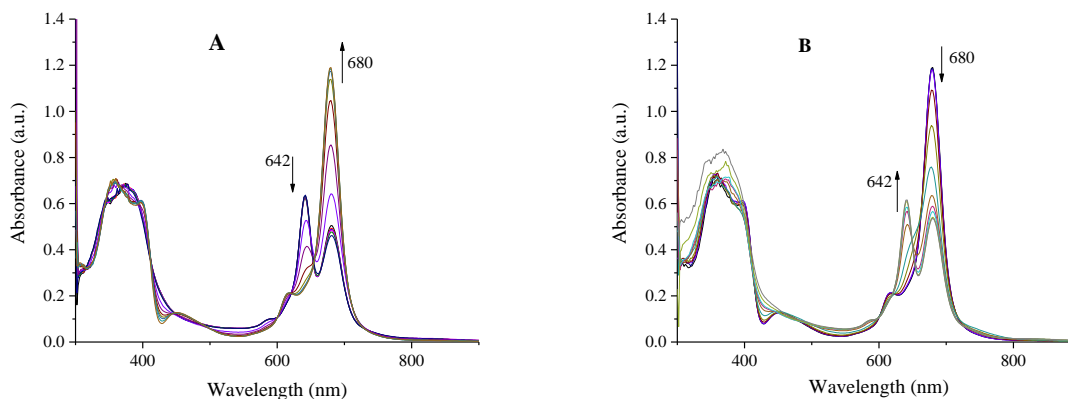
**Figure S18.** UV-vis spectroscopic changes seen upon addition of tetrabutylammonium fluoride to a solution of **2c** in pyridine.



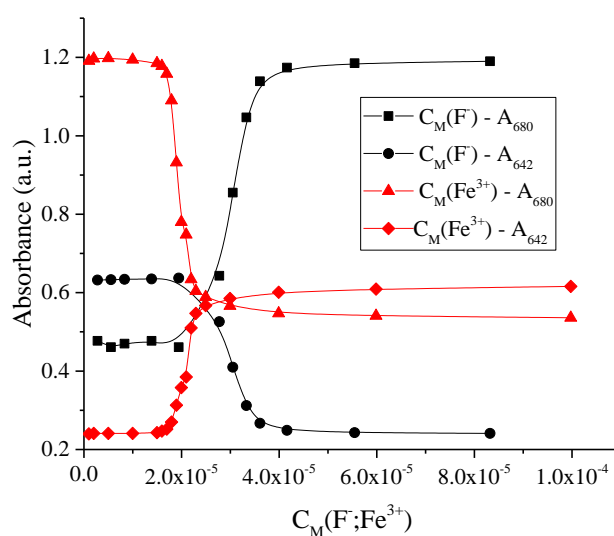
**Figure S19.** Change in absorbance at 679 and 641 nm seen upon titration of **2c** with tetrabutylammonium fluoride in pyridine. Concentrations are in mol L<sup>-1</sup>.



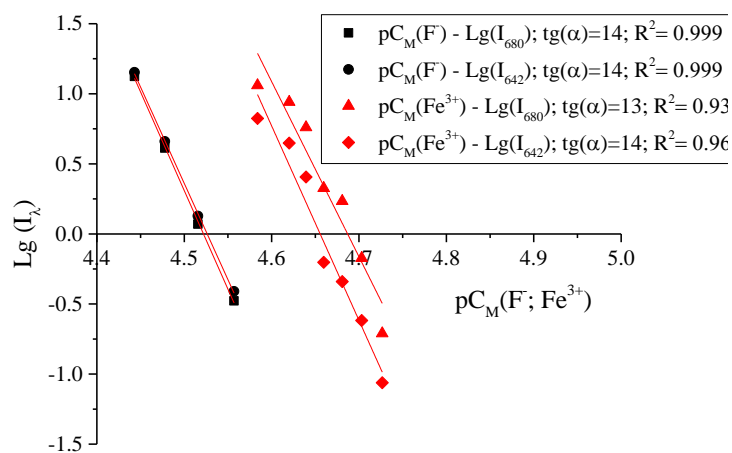
**Figure S20.** Plots of the indicator concentration ratio for **2c** at 679 and 641 nm vs. the negative log of the tetrabutylammonium fluoride concentration.



**Figure S21.** UV-vis spectroscopic changes during dissociation of dimeric form of **2c** in pyridine seen upon addition of tetrabutylammonium fluoride (**A**) and the following reverse dimerization process upon addition of  $\text{FeBr}_3$  (**B**).

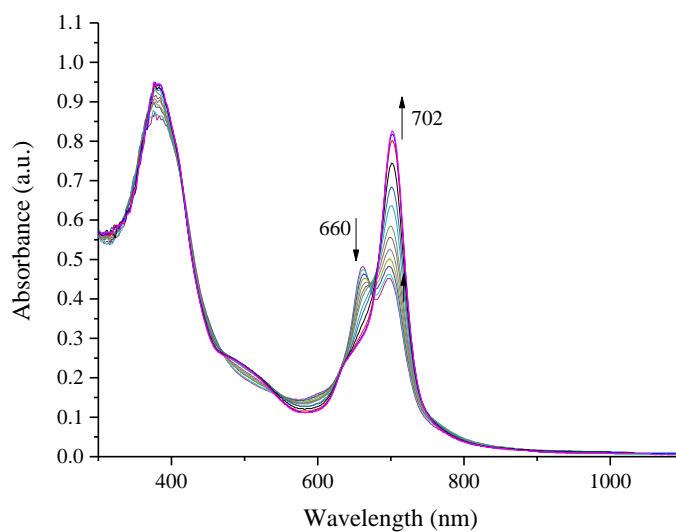


**Figure S22.** Change in absorbance at 680 and 642 nm seen upon titration of **2c** with tetrabutylammonium fluoride in pyridine and upon titration of the resulting solution with  $\text{FeBr}_3$ . Concentrations are in  $\text{mol L}^{-1}$ .

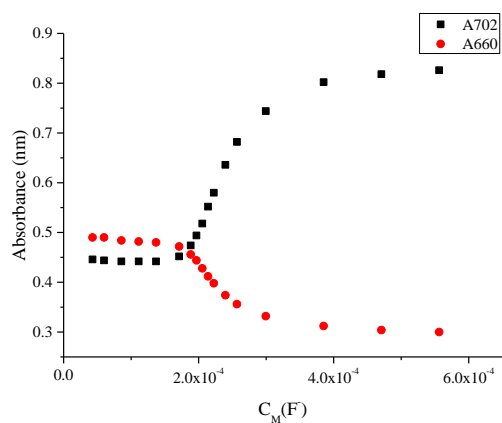


**Figure S23.** Plots of the indicator concentration ratio for **2c** at 680 and 642 nm vs. the negative log of the tetrabutylammonium fluoride or  $\text{FeBr}_3$  concentration.

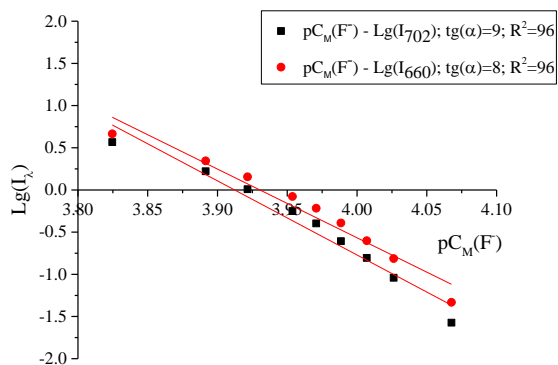
Complex **2b** in DMSO



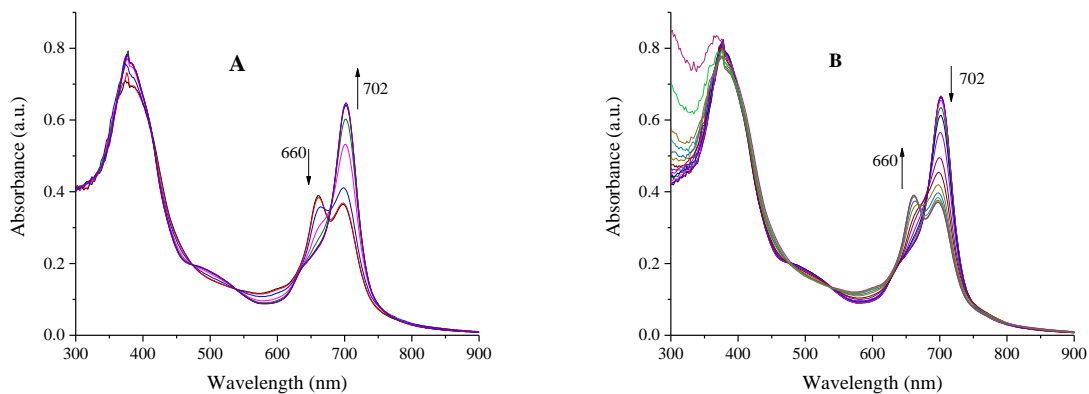
**Figure S24.** UV-vis spectroscopic changes seen upon addition of tetrabutylammonium fluoride to a solution of **2b** in DMSO.



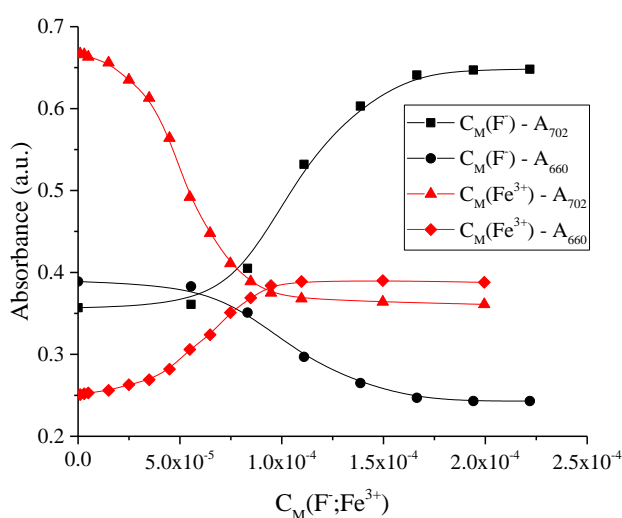
**Figure S25.** Change in absorbance at 702 and 660 nm seen upon titration of **2b** with tetrabutylammonium fluoride in DMSO. Concentrations are in mol L<sup>-1</sup>.



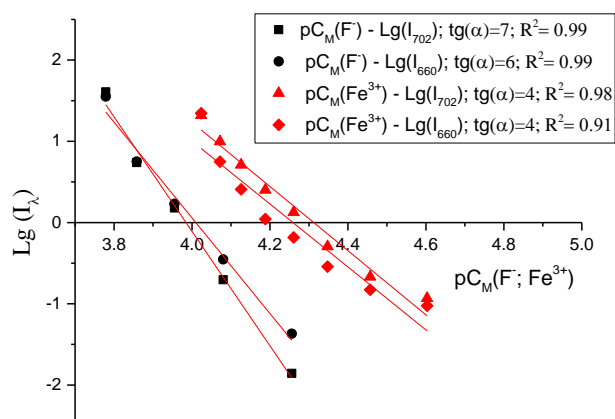
**Figure S26.** Plots of the indicator concentration ratio for **2b** at 702 and 660 nm vs. the negative log of the tetrabutylammonium fluoride concentration.



**Figure S27.** UV-vis spectroscopic changes during dissociation of dimeric form of **2b** in DMSO seen upon addition of tetrabutylammonium fluoride (**A**) and the following reverse dimerization process upon addition of  $\text{FeBr}_3$  (**B**).

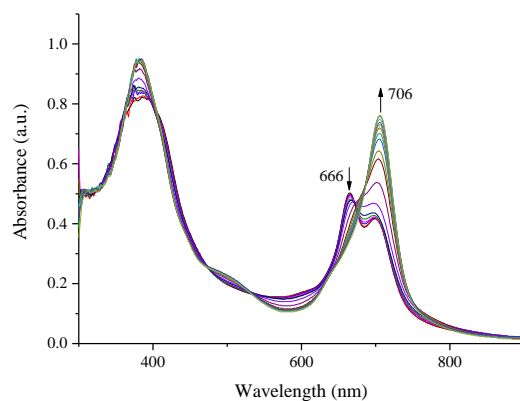


**Figure S28.** Change in absorbance at 702 and 660 nm seen upon titration of **2b** with tetrabutylammonium fluoride in DMSO and upon titration of the resulting solution with  $\text{FeBr}_3$ . Concentrations are in  $\text{mol L}^{-1}$ .

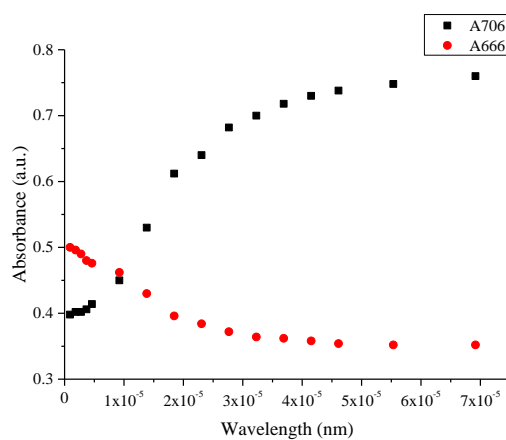


**Figure S29.** Plots of the indicator concentration ratio for **2b** at 702 and 660 nm vs. the negative log of the tetrabutylammonium fluoride or  $\text{FeBr}_3$  concentration.

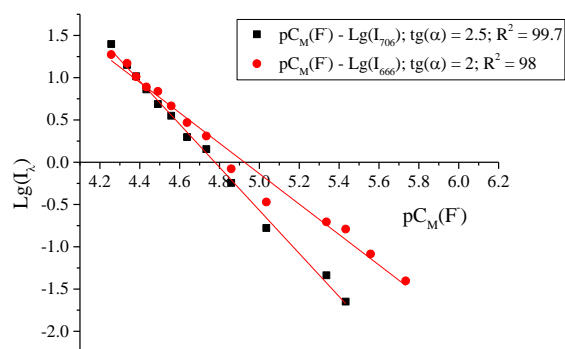
### Complex **2b** in pyridine



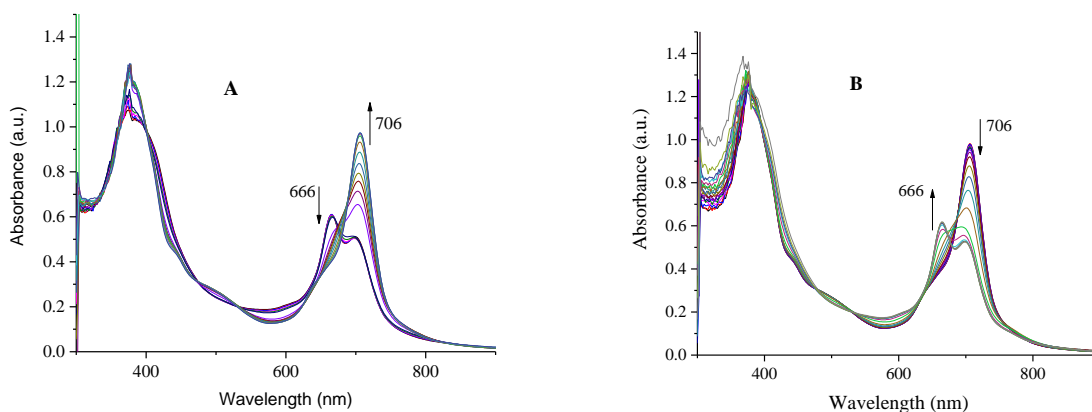
**Figure S30.** UV-vis spectroscopic changes seen upon addition of tetrabutylammonium fluoride to a solution of **2b** in pyridine.



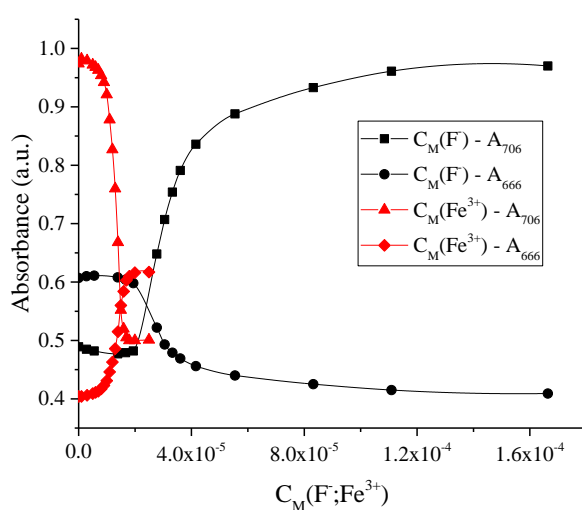
**Figure S31.** Change in absorbance at 706 and 666 nm seen upon titration of **2b** with tetrabutylammonium fluoride in pyridine. Concentrations are in mol L<sup>-1</sup>.



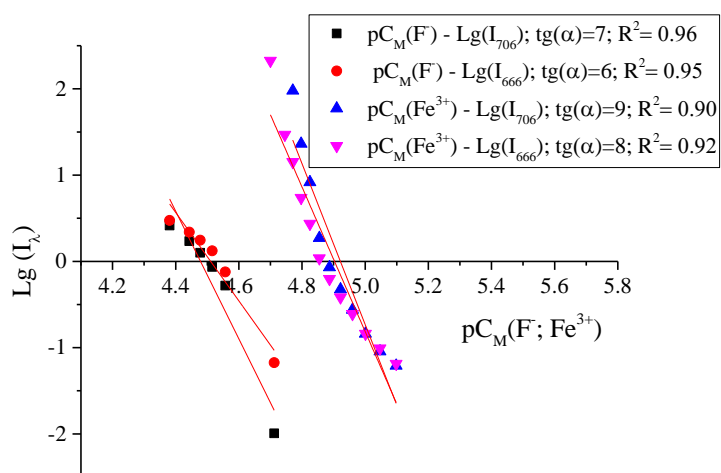
**Figure S32.** Plots of the indicator concentration ratio for **2b** at 706 and 666 nm vs. the negative log of the tetrabutylammonium fluoride concentration.



**Figure S33.** UV-vis spectroscopic changes during dissociation of dimeric form of **2b** in pyridine seen upon addition of tetrabutylammonium fluoride (**A**) and the following reverse dimerization process upon addition of  $\text{FeBr}_3$  (**B**).



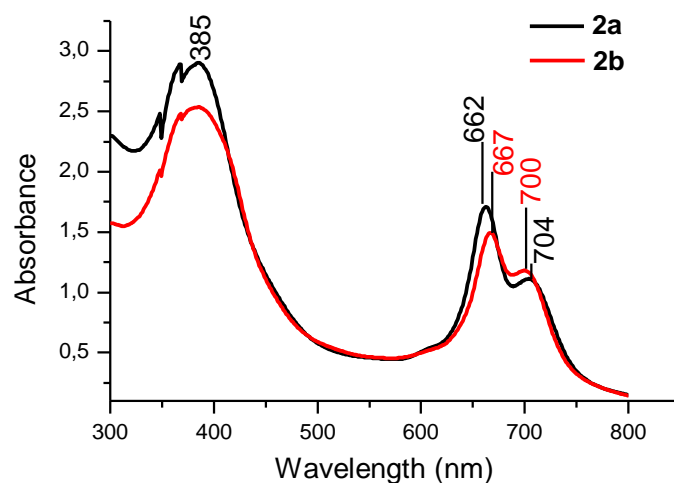
**Figure S34.** Change in absorbance at 706 and 666 nm seen upon titration of **2b** with tetrabutylammonium fluoride in pyridine and upon titration of the resulting solution with  $\text{FeBr}_3$ . Concentrations are in  $\text{mol L}^{-1}$ .



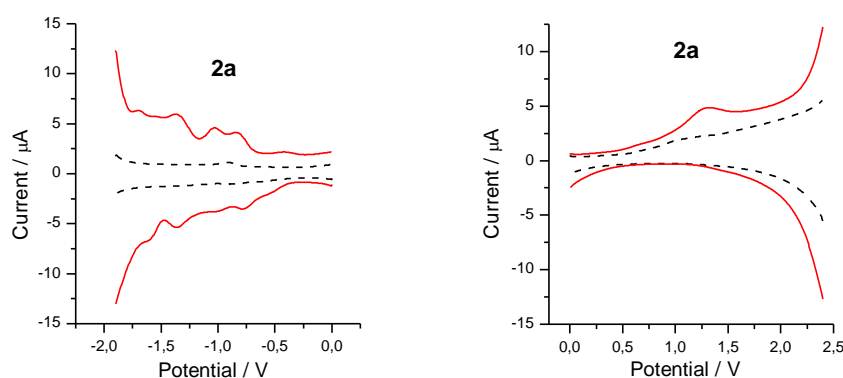
**Figure S35.** Plots of the indicator concentration ratio for **2b** at 706 and 666 nm vs. the negative log of the tetrabutylammonium fluoride or  $\text{FeBr}_3$  concentration.

## Electrochemistry

Electrochemical analyses of **2a** and **2b** were carried out in pyridine containing 0.1 M [TBA][BF<sub>4</sub>] as the supporting electrolyte. Under these conditions the complexes exist in their dimeric forms as illustrated in Figure S36. One broad irreversible oxidation peak was observed at a potential of 0.804 and 0.777 V (vs. SCE) for **2a** and **2b**, respectively. Reductive scans revealed more complex electrochemistry; up to five reversible redox processes were observed (Table S1, Figure S37). Such behavior is consistent with the proposed dimeric nature of the complexes, which can lead to a splitting of redox transitions similar to what is seen in the case of double-decker sandwich complexes stabilized by a central lanthanide cation.<sup>6-8</sup> The single broad oxidation peak could result from two closely located irreversible redox transitions. Complexes **2a** and **2b** appear to be noticeably more stable towards oxidation than monomeric phthalocyanine complexes<sup>9</sup> and sandwich-type double-decker systems.<sup>7,8</sup> The  $\Delta R_{21}$  ( $R_2 - R_1$ ) and  $\Delta R_{43}$  ( $R_4 - R_3$ ) values are larger for **2a** than for **2b**, which is as expected given the greater Q-band splitting seen in the UV-vis spectrum (cf. Figures 2 and S36). The reduction potentials  $R_1$ ,  $R_2$ , and  $R_3$  for **2b** were slightly shifted to more negative values relative to **2a**, meaning that the reduction of complex **2b** is more difficult. Such a finding is as expected given the stronger electron-donating effect of the substituents present in **2b**.



**Figure S36.** UV-vis spectra recorded for samples of **2a** and **2b** in pyridine in the presence of supporting electrolyte. The concentrations of **2a** and **2b** were both ca. 0.1 mM; the cuvette path length was 1 mm.



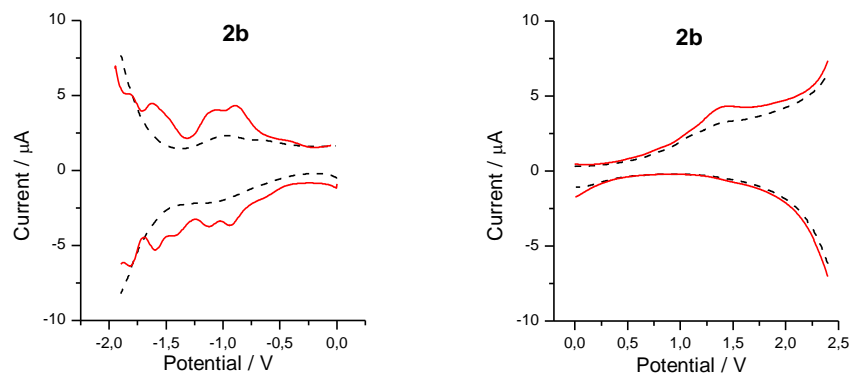


**Figure S37.** SWVA of complexes **2a** and **2b** in pyridine containing 0.1 M [TBA][BF<sub>4</sub>]. Amplitude, 50 mV; frequency, 10 Hz; step potential, 5 mV;  $E_{1/2}(\text{ferrocene}^+/\text{ferrocene}) = 0.49$  V under these experimental conditions.

**Table S1.** Reduction potentials for **2a** and **2b** in pyridine (values vs. SCE<sup>a</sup>)

	Ox <sub>1</sub> <sup>b</sup>	Red <sub>1</sub>	Red <sub>2</sub>	Red <sub>3</sub>	Red <sub>4</sub>	Red <sub>5</sub>
<b>2a</b>	1.294	-0.790	-1.016	-1.356	-1.646	-
<b>2b</b>	1.267	-0.883	-1.073	-1.433	-1.593	-1.793

<sup>a</sup>  $E_{1/2}(\text{Fc}^+/\text{Fc}) = 0.49$  V. <sup>b</sup> Irreversible process; the value of the peak potential is given.

## In Vitro and in Vivo Toxicity Tests

Compounds **2a,b** were converted into water-soluble forms by co-solvation with polyvinylpyrrolidone (PVP) for biological testing.

Cell viability was recorded as dehydrogenase activity as inferred from 3-(4,5-dimethylthiazol-2-yl)-2,5-diphenyltetrazolium bromide (MTT) assays.<sup>10</sup> Briefly, the SH-SY5Y cells or primary culture of rat cerebellar granule cells were incubated with the test compounds or equivalent volume of vehicle (less than 1% of the whole volume of medium under the layer of cells) for 24 h. Then, 20  $\mu\text{L}$  of MTT (2 mg mol<sup>-1</sup> in PBS) were added to each well and the cells were incubated at 37°C for 2 h. The supernatants were aspirated carefully, 200  $\mu\text{L}$  of DMSO were added to each well to dissolve the precipitate, and the absorbance was measured at 570 nm using a microplate reader Victor (Perkin Elmer).

Acute intraperitoneal toxicity of complexes **2a** and **2b** was determined using male hybrid mice BDF1 (weighing 20–22 g) by injection of single doses of 25, 50, 100, and 150 mg kg<sup>-1</sup> body weight, respectively. Mice were kept under specific pathogen-free conditions; water and food were provided *ad libitum*. All animals were observed for clinical signs of toxicity within the first 30 min following dose administration, and then – with an interval of 1–4 h and further – once daily for 14 days. No deaths were registered during the 14 day study periods associated with either complex. The data obtained were plotted as a dose–effect curve, from which the acute toxicity values (MTD, LD<sub>50</sub> and LD<sub>100</sub>) of complexes **2a** and **2b** were determined.

**Table S2.** Acute toxicity studies of compounds **2a** and **2b** as determined using mal hybrid mice BDF1.

Compound	Injected dose, mg kg <sup>-1</sup>	Number of animals per group	Number of deaths at day 14 after injection
PVP	100	6	0
	250	6	0
	500	6	0
	750	6	0
	1500	6	0
	3750	6	0
	7500	6	0
<b>2a</b>	10	6	0
	50	6	0
	100	6	0
	150	6	0
<b>2b</b>	10	6	0
	50	6	0
	100	6	0
	150	6	0

## References

1. P. A. Tarakanov, M. P. Donzello, O. I. Koifman and P. A. Stuzhin, *Macroheterocycles* 2011, **4(3)**, 177-183
2. P. Evans, *Acta Crystallogr., Sect. D: Biol. Crystallogr.*, 2005, **D62**, 72-82.
3. T. G. Battye, O. Kontogiannis L Fau - Johnson, H. R. Johnson O Fau - Powell, A. G. W. Powell Hr Fau - Leslie and A. G. Leslie, *Acta Crystallogr., Sect. D: Biol. Crystallogr.*, 2011, **D67**, 271-281.
4. A. L. Spek, *Journal*, 2006.
5. G. M. Sheldrick, *Acta Crystallographica Section A*, 2008, **64**, 112-122.
6. E. N. Tarakanova, S. A. Trashin, A. O. Simakov, T. Furuyama, A. V. Dzuban, L. N. Inasaridze, P. A. Tarakanov, P. A. Troshin, V. E. Pushkarev, N. Kobayashi and L. G. Tomilova, *Dalton Trans.*, 2016, **45**, 12041-12052.
7. V. E. Pushkarev, A. Y. Tolbin, N. E. Borisova, S. A. Trashin and L. G. Tomilova, *Eur. J. Inorg. Chem.*, 2010, DOI: 10.1002/ejic.201000511, 5254-5262.

8. P. Zhu, F. Lu, N. Pan, Dennis P. Arnold, S. Zhang and J. Jiang, *Eur. J. Inorg. Chem.*, 2004, **2004**, 510-517.
9. E. Ough, T. Nyokong, K. A. M. Creber and M. J. Stillman, *Inorg. Chem.*, 1988, **27**, 2724-2732.
10. M. Nikš and M. Otto, *J. Immunol. Methods*, 1990, **130**, 149-151.